JM3 Journal of Micro/Nanopatterning, Materials, and Metrology

RESEARCH PAPER

Interface sharpness in stacked thin film structures: a comparison of soft X-ray reflectometry and transmission electron microscopy

Richard Ciesielski,[a,*] Janusz Bogdanowicz,[b] Roger Loo,[b,d] Yosuke Shimura,[b] Antonio Mani,[c] Christoph Mitterbauer,[c] Michael Kolbe,[a] and Victor Soltwisch[a]

[a]Physikalisch-Technische Bundesanstalt, Berlin, Germany
[b]Imec, Leuven, Belgium
[c]Thermo Fisher Scientific, Eindhoven, The Netherlands
[d]Ghent University, Department of Solid-State Sciences, Ghent, Belgium

ABSTRACT. **Background:** A key element of semiconductor fabrication is the precise deposition of thin films. Among other aspects, the quality of interfaces between different materials plays a crucial role for the success of further processing steps.

Aim: We here present a combined quantitative study of soft X-ray reflectometry measurements compared to scanning transmission electron microscopy and energy dispersive X-ray spectroscopy (STEM-EDX) on stacked thin film samples of silicon and silicon-germanium (SiGe).

Approach: The thin film structures feature two distinct germanium concentrations in the SiGe layers and are produced for complementary field-effect transistor applications. We use synchrotron-based, angle-, and energy-resolved broadband reflectance to investigate the sharpness of the layer interfaces, which is accessible through rigorous modeling of the acquired data. Complementary, the samples are investigated using STEM-EDX on thin lamellas across the interfaces, which give a direct representation of the interface sharpness through the varying germanium content.

Results: Layer thicknesses and interface properties are studied with the two methods. As a side-product of the measurement, the optical constants of the different SiGe compounds are determined and reported.

Conclusions: We find a very high correlation of the retrieved values between both methods and discuss their comparability and limits.

Keywords: EUV reflectometry; scanning transmission electron microscopy and energy dispersive X-ray spectroscopy; SiGe; interface sharpness; layer intermixing

Paper 24013SS received Mar. 26, 2024; revised Jun. 25, 2024; accepted Jul. 9, 2024; published Aug. 23, 2024.

1 Introduction

As the semiconductor industry progresses to more complex and smaller transistor designs using extreme ultaviolet (EUV) lithography, the accompanying metrology must constantly refine existing methods and develop new ones to keep up with the rapid development. One of the foundations for further manufacturing steps is precise thin-film deposition. The determination of the layer thicknesses for thin-film structures is typically done using X-ray reflection (XRR), optical

*Address all correspondence to Richard Ciesielski, richard.ciesielski@ptb.de

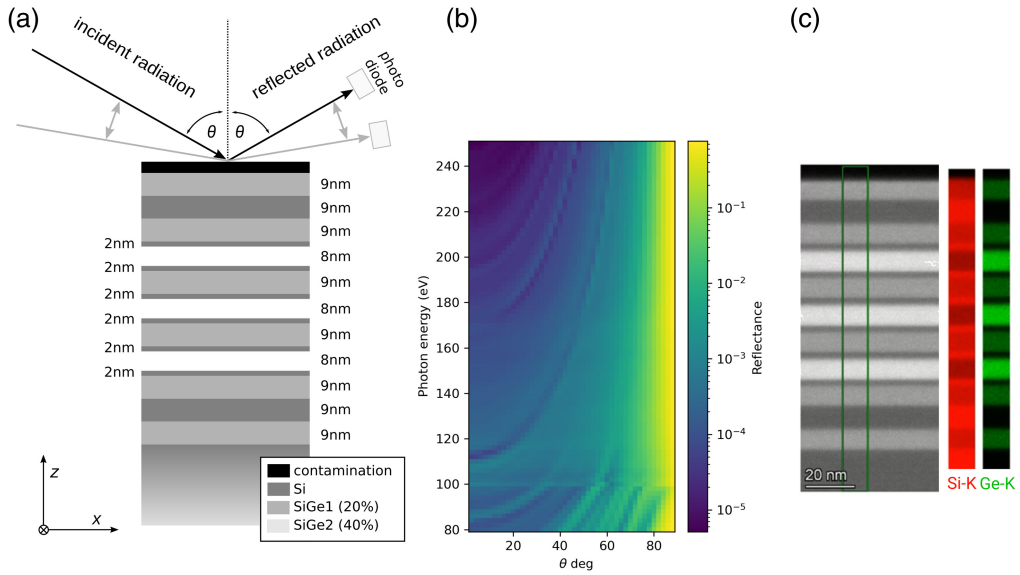

Fig. 1 Sample material and central measurements. (a) The sample consists of several layers of silicon and silicon-germanium as used for CFET devices. Reflectometry measurement principle: monochromatic radiation in the soft X-ray regime is reflected off the sample surface and detected by a photodiode as a function of the angle of incidence θ while the photon energy is scanned. (b) Angle-resolved reflectance data in the photon energy range of 80 eV...250 eV and from grazing incidence to near-normal. (c) STEM-EDX data of the sample: dark field signal and EDX data for the silicon and germanium K-edge.

methods like ellipsometry, or transmission electron microscopy (TEM).[1] The study of buried interfaces, on the other hand, still remains challenging. For devices with shrinking dimensions, the role of interfaces becomes more and more important since they determine the performance to a large extent, but also in other areas, such as quantum computing, the role of interfaces is central. Therefore, the importance of interface metrology is rising. Besides electron microscopy methods,[2,3] atom probe tomography has successfully been used to quantify the extent of intermixing regions at layer interfaces.[4,5] The next step in the device evolution is the complementary field-effect transistor (CFET), which is considered for beyond 1 nm technology nodes.[6] In the monolithic fabrication scheme, n- and p-MOS transistors are built on the same wafer. It starts with the epitaxial deposition of a complex SiGe/Si multilayer-stack with at least two different germanium concentrations [Fig. 1(a)]. Later, the germanium-rich SiGe layers would be replaced by an isolating dielectric.

This work[7] compares our studies of blanket layer stacks (before lithography steps and etching) as used for CFET devices using broadband angular-resolved soft X-ray/EUV reflectometry and scanning transmission electron microscopy combined with spectroscopic mapping (STEM-EDX). Both methods can determine the layer structure of a sample and quantify the extent of intermixing layers at the interfaces between different materials, commonly denoted as interface sharpness or interface abruptness. This quantification turns out to be central for the comparison of both methods. Reflectometry is non-destructive but model-based and requires a large sample area, whereas STEM-EDX is an imaging technique that needs lamella cuts of the sample. We find remarkable agreement between both methods and discuss their applicability, advantages, and disadvantages. Furthermore, our X-ray reflectometry study yields the optical constants of the two SiGe variants. As SiGe layers have further applications, e.g., in strain engineering, as sacrificial layers,[8] or for quantum computing,[9] the precise knowledge of their material properties is critical. We present the optical constants of two SiGe materials with varying germanium content that were retrieved from the soft X-ray reflectometry data.

2 Sample Material

The samples investigated consist of several layers of silicon and two silicon-germanium (SiGe) alloys, as used for monolithic CFET device studies.[10,11] A sketch of the sample with the nominal

layer thicknesses is presented in Fig. 1(a). The layers were epitaxially grown on an undoped silicon wafer in a production compatible ASM Intrepid™ RP-CVD cluster tool using the growth schemes described elsewhere[12] under conventional temperature and conventional precursors. The indicated topmost layer is not an original part of the sample, but accounts for two effects: a thin native oxide layer and some contamination that is formed as a result of the transport of the samples under ambient conditions. There are two variants of SiGe in the sample: SiGe1 with a nominal germanium content of 20% and SiGe2 with a nominal germanium content of 40%. Wafer pieces of several square centimeters area were used for the measurements.

3 Soft X-ray Reflectometry Measurements

3.1 Experimental Setup and Measurements

Reflectometry measurements were performed at the soft X-ray beamline[13,14] in the laboratory of the Physikalisch-Technische Bundesanstalt at the synchrotron radiation facility BESSY II in Berlin. It provides s-polarized (>98%) monochromatic radiation ($E/\Delta E \approx 400$) with low divergence (<1 mrad). The goniometer allows for precise six-axis alignment of the samples and features full lubricant-free mechanics to minimize contamination of the samples through hydrocarbons from the bearings.[15] Radiation reflected off the sample is measured by a GaAsP photodiode, scanning the angle-of-incidence θ in the range of $1...89°$ and the photon energy in the range of $80...250$ eV. The raw measurement data are presented in Fig. 1(b), with an average relative measurement uncertainty of 0.8%. At grazing incidence $\theta \approx 90°$, the reflectivity of the sample approaches 1 while it drops to $10^{-3}...10^{-5}$ at near normal $\theta \approx 0°$, depending on the photon energy. Several interference fringes are visible throughout the data set, shifting with the photon energy. Around 100 eV, a sudden feature can be seen that stems from the silicon L-edges. A more detailed account of the measurement and the data fitting procedure is given elsewhere.[16–18]

3.2 Model Fit

We use a transfer matrix approach[16,19–21] to calculate the reflectivity of a specific sample as a function of its geometrical parameters and of the optical constants of the materials. This method is based on the Fresnel equations and Beer's law to describe the reflectivity and transmission of the individual interfaces and layers. Diffuse scattering from the interfaces is taken into account by a Névot-Crocet/Debye-Waller factor that reduces the reflectivity according to Refs. 20 and 22

$$r_{i/i-1} \propto \exp\left[-\frac{1}{2}(k_{z,i} \pm k_{z,i-1})^2 \cdot \sigma_{i/i-1}^2\right], \tag{1}$$

where $r_{i/i-1}$ is the Fresnel reflection coefficient of the electric field of the interface between materials i and $i-1$, $k_{z,i}$ is the out-of-plane component of the wave vector within material i, and $\sigma_{i/i-1}$ is an interface parameter for the interface between material i and $i-1$ in units of length. The sign ($\pm$) is chosen based on whether the wave is travelling upward or downward within the matrix method (see 16 for details). The interface parameter $\sigma_{i/i-1}$ describes the strength of the signal reduction due to diffuse scattering, caused by two distinct effects: lateral roughness and interface intermixing.[22] Based on the specular reflectance only, the two effects are indistinguishable.[23] In the present case, the dominant effect is interface intermixing (c.f. Sec. 4) and in this situation, the parameter $\sigma_{i/i-1}$ measures the width of the intermixing layer.[22] Therefore, interface sharpness is high, when $\sigma_{i/i-1}$ is low and vice versa (c.f. discussion in Sec. 5.1).

The model is used for a fit to the experimentally obtained data. There are two kinds of parameters in the model: global parameters, which are valid for all energies. These are the layer thicknesses l_i, interface parameters $\sigma_{i/i-1}$, the density of silicon, and a small offset in the angle of incidence θ. Then, there are energy-dependent parameters, which are the optical constants (δ, β) for the SiGe layers and the contamination. The model assumes that tabulated data for the optical constants of silicon, slightly scaled by the material density, can be used.[24] The full model consists of 18 individual layers and 19 interfaces. We assume that the 2 nm thin layers of silicon have a density ρ_1 that is slightly different from the density of the thicker layers and the substrate ρ_2; therefore, these two densities are fit parameters, too. Together with an offset of the angle of

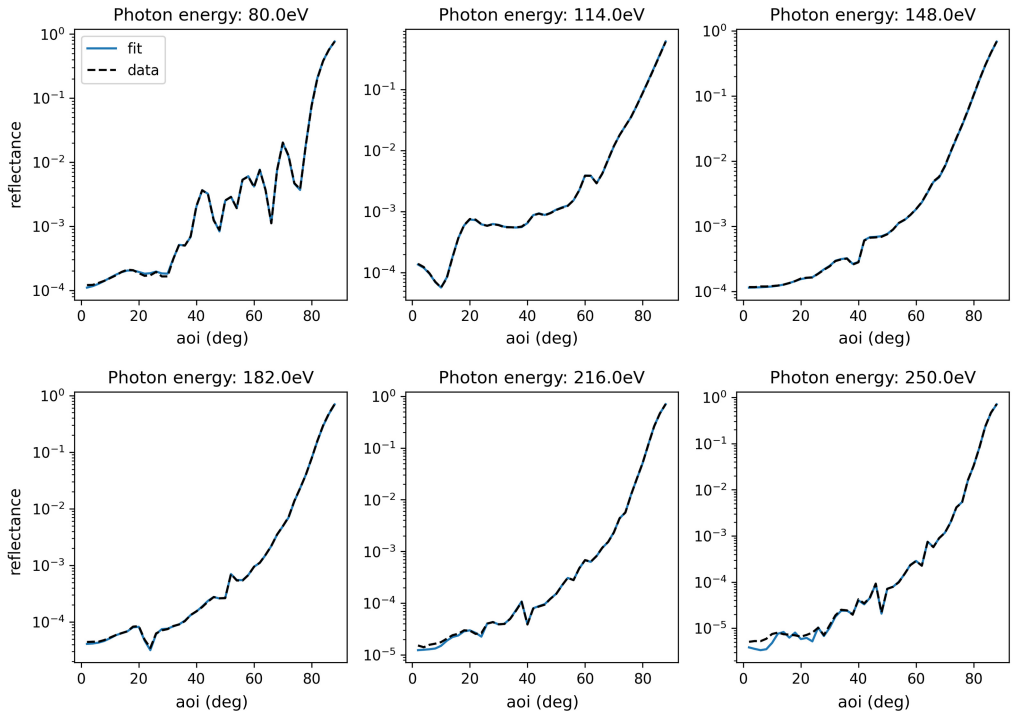

Fig. 2 Fit results of the soft X-ray reflectometry data from Fig. 1(b) for selected photon energies throughout the measured spectrum. Since the blanket layer stack is complex, the measured and calculated curves show many features. The agreement of fit and data is overall excellent, and deviations occur only at low angles of incidence (aoi) for the higher photon energies, where the total reflectance is on the order of 10^{-5}.

incidence, these are 40 global parameters. The model further assumes that all of the SiGe1 layers in the stack share identical optical constants and that the same is true for all the SiGe2 layers. At 85 measured energies, the number of energy-dependent parameters $(\delta_i(E), \beta_i(E))$ adds up to $2 \times 2 \times 85 = 340$.

While the energy-dependent optical constants were calculated using least square optimization,[25] we used a global optimization algorithm[26] to determine a set of global parameters that describe the data set well.[16] These parameters were used as initial guess for a Markov-Chain Monte-Carlo sampling over the global parameters.[27,28] The statistics show that all parameters are sufficiently independent. The resulting fit to the data is presented in Fig. 2. The agreement of fit and data is overall excellent, deviations occur only at low angles of incidence for the higher photon energies, where the total reflectance is on the order of 10^{-5}. Through this fit, a set of layer thicknesses l_i and interface parameters $\sigma_{i/i-1}$ was determined for the blanket layer stack, as well as the optical constants of the two SiGe variants. The geometrical parameters are discussed in Sec. 5.1, and the optical constants are discussed in Sec. 5.2. The fit results for the silicon densities are: $\rho_1 = 2.345$ g/cm^3, $\rho_2 = 2.362$ g/cm^3, which is very close to the tabulated value of $\rho = 2.329$ g/cm^3 for crystalline silicon. The differences thereof probably reflect the accuracy of the fit rather than actual differences in the layers. The fitted offset of the angle of incidence amounts to 0.006 deg, which is plausible given the accuracy of the used goniometer axis.

4 TEM-based Measurements

4.1 Experimental Setup and Measurements

Lamellae of 35 to 45 nm thickness were prepared by means of a manually operated Helios5 UX FIB/SEM dual beam system. A protective capping layer of tungsten was deposited. STEM and STEM-EDX micrographs were acquired at ThermoFisher Scientific by means of a spectra ultra transmission electron microscope. The system was equipped with a monochromated X-FEG (not excited), a piezo stage, a PantherSTEM™ detector, and an UltraX™ EDX detector. Figure 1(c)

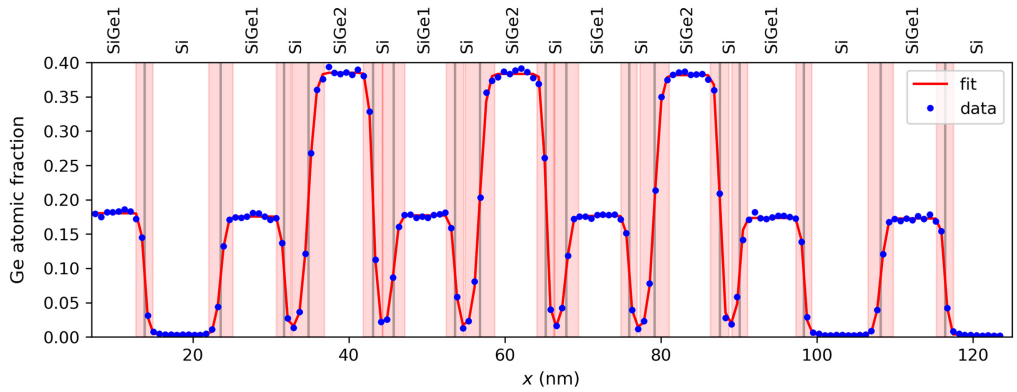

Fig. 3 Measured germanium content through the sample cross section determined by STEM-EDX (blue dots). The silicon substrate begins at $x > 115$ nm. The red line shows a model fit according to Eq. (2). The vertical gray lines point to the positions of the layer interfaces and the red shaded areas show the extent of the associated intermixing layers and correspond to $\pm 2\sigma$.

presents STEM-EDX data of a single lamella cut out of the sample where the different layers are clearly visible. We observe that the transition between the individual layers are not atomically sharp but that there is a considerable transition region. Laterally, the interfaces show no sign of roughness on the length scales observed here. Although it is common practice to determine layers thicknesses by analyzing HAADF-STEM or TEM micrographs, we decided to focus on the chemical nature of the interfaces considered; therefore, we utilized the STEM-EDX signals for determining the thickness and the extent of the intermixing zones between the layers. Therefore, the STEM-EDX signal was processed through ThermoFisher Scientific's Velox™ software. In this environment, the STEM-EDX map of the lamella is quantified over an X by Y window using an empirical model consisting in a three-parameter Bethe-Heitler function, which is used to fit the entire measured spectrum. Applying a background model, such spectrum based quantification was applied to a line scan over the entire length of the stack. The data acquired in this way are shown for the germanium atomic fraction as blue dots in Fig. 3. Two more lamellas of the same sample were used to generally verify the results but have not undergone the entire data evaluation procedure. The measured atomic fraction of germanium in SiGe1 is 18.7% and in SiGe2 40.5%.

4.2 Model Fit

To determine the layer thicknesses and to extract the interface sharpness, we use the following model equation to describe the EDX data:

$$\text{Ge atomic fraction}(x) = \sum_i \frac{a_i}{2} \cdot \left(1 + \text{erf}\left(\frac{x - x_i}{\sigma_i}\right)\right) + b, \tag{2}$$

where the measured atomic fraction of germanium throughout the sample is modeled through a sum of error functions erf() with suitable amplitudes a_i, center positions x_i, widths σ_i, and an additional offset b. The index i counts the interfaces, starting at the top. The error functions were chosen to describe the transition of the atomic fraction between the individual layers, which are not atomically sharp transitions but softened up through intermixing processes. We do not observe any sign of an asymmetric transition within the given spatial resolution of the TEM images, so the symmetric error function as model curve seems plausible. As such, the parameter σ describes the extent of the intermixing identically to the theory for reflectometry in Eq. (1) and is likewise an inverse measure of the interface sharpness. Equation (2) can analogously be formulated to describe the atomic fraction of silicon in this layer stack. The fit to the germanium data in Fig. 3 (red line) shows that this model describes the measured data very well. Out of these results, we obtained the layer thicknesses $l_i = x_{i+1} - x_i$ and the widths of the intermixing regions σ_i for the entire sample. The center positions of the interfaces x_i are denoted by vertical, gray lines, and the widths of these interfaces are shown as red shaded areas, covering $\pm 2\sigma$. Even though the silicon layers in between the SiGe layers are very thin ($\approx$2 nm), they are well resolved in the TEM data and can be modeled through Eq. (2).

5 Results and Discussion

5.1 Comparison of Soft X-ray and STEM-EDX Results: Layer Thicknesses, Interface Sharpness, and Applicability

In Fig. 4, we present the geometrical parameters of the sample as determined by soft X-ray reflectometry and STEM-EDX. Figures 4(a) and 4(c) show the film thicknesses and their correlation where we find an excellent agreement between the two methods, which has also been verified on a second sample (data not shown). This demonstrates the general applicability of both, broadband soft X-ray reflectometry and STEM-EDX to the problem. Note that the measured thicknesses deviate from the design values, given in Fig. 1(a) by ± 1 nm.

Figures 4(b) and 4(d) compare the retrieved interface sharpness parameters σ. We find that both methods show the same trend over the layer stack and that they compare well, although STEM-EDX retrieves generally higher values of σ than reflectometry, which means that reflectometry detects slightly sharper layer transitions than STEM-EDX. The difference between the determined layer thicknesses and sharpness of both methods is in the range of a few angstroms. It is possible that these small differences originate from the fact that different sample positions of

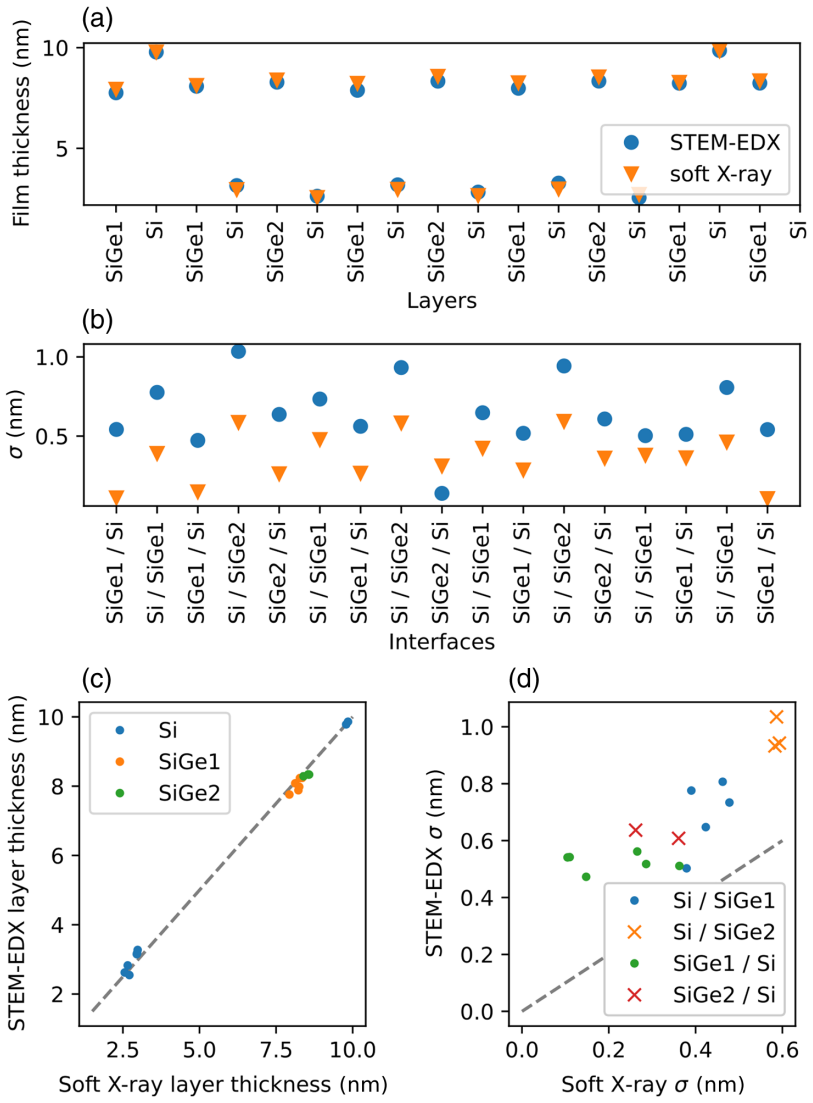

Fig. 4 Comparison of soft X-ray-based and STEM-EDX-based determination of film thicknesses and interface intermixing σ. In panels (a) and (c), it is shown that the film thicknesses correlate very well for all layers. In panels (b) and (d), it is visible that the interface intermixing parameters, determined through STEM-EDX follow the same trend as those determined through reflectometry but feature slightly higher values.

the 300 mm wafer were probed, where deviations on an angstrom-level can occur over lateral distances of centimeters. Furthermore, the STEM-EDX data represent only a small fraction on the sample in the range of tens of nanometers, whereas the reflectometry results represent a spatial average in the range of a few square millimeters, due to the nature of the measurements. Therefore, it cannot be excluded that the small observed differences stem from spatial inhomogeneities of the sample itself. The labels in Fig. 4(b) refer to the interfaces from top to bottom, such that "Si/SiGe1" refers to an interface where a silicon layer had been deposited on top of a SiGe1 layer. Detected by both methods are two remarkable trends in σ that give insight into the details of the layer structure: first we see that SiGe on top of Si gives sharper interfaces (lower σ) than Si on top of SiGe. Second, the interfaces containing SiGe1 are generally sharper than those, containing SiGe2.

As explained earlier, the σ-value in reflectometry is a measure of interface sharpness and roughness.[20] This number is based on the theory that either the lateral displacement of the interface's position varies stochastically or that there is a region of layer intermixing instead of perfectly well defined interfaces.[22] Our TEM study shows that the interfaces between the layers can be well described by a smooth transition of the germanium/silicon content, following an error function. It further shows that lateral roughness can be neglected for the present case because its amplitude is far smaller than the extent of the intermixing region, visible in the dark field TEM image in Fig. 1. Therefore, we can directly compare the determined values of $\sigma_i^{\text{refl.}}$ from Eq. (1) with those determined through STEM-DEX σ_i^{EDX} in Eq. (2), because they describe the same quantity.

In the present case, the overall quality of the blanket layer stacks was very high in the sense that the layers were crystalline, spatially homogeneous, not porous, and very smooth, due to the epitactic deposition process. This is advantageous both for TEM lamella preparation and the data evaluation of the reflectometry measurements and makes the samples ideally suited for this kind of comparison. Both measurement methods come with advantages and disadvantages. Soft X-ray reflectometry is a non-destructive method that gives insight into averaged sample properties. It is sensitive to the surface and buried layers and interfaces down to approximately 100 nm depth, depending on the materials and the wavelengths used. It requires a relatively large sample area due to the increased beam footprint at grazing incidence and can only provide layer thickness and interface properties through model-based reconstruction. This modeling either has to include a fit of the optical constants, as done in the present work, or needs precise knowledge of the properties of the materials in question. STEM-EDX, as an imaging technique, directly provides the sample geometry and the material distribution. It gives local, but high-resolution information about the sample. The method is destructive since lamellas must be cut out of the sample. Both methods require advanced equipment, but STEM-EDX is typically more easily accessible than synchrotron-based reflectometry.

5.2 Optical Constants of SiGe

An additional result of the reflectance data fit were the optical constants of the two SiGe variants, which we present in Fig. 5 alongside a comparison to existing data of pure silicon and pure germanium.[24] Appendix A gives the full list of the retrieved optical constants for reference. Germanium's extinction coefficient β is monotonically decreasing with increasing energy, and its dispersion coefficient δ features a very broad maximum around 180.1 eV from the M3 edge.[24] Silicon, on the other hand, has a prominent absorption edge from its L-edges at 99.2 eV (L2) and 99.8 eV (L3),[24] visible around 100 eV in the data. This feature is also observed in the optical constants of both SiGe variants. Without further data evaluation, it is visible that SiGe1 (blue line) falls between the optical constants of pure silicon and pure germanium. When the optical constants of SiGe1 are fitted to a mixture of the displayed tabulated data of silicon and germanium, an atomic fraction of 17.7% germanium is determined at a RMSE of $5 \cdot 10^{-4}$, showing that the optical constants of this material can be predicted reasonably well from the materials of its constituents. For SiGe2, this works only in a qualified sense. Here, the obtained atomic fraction is 40.3% at a RMSE of $1.4 \cdot 10^{-3}$, which means that the prediction of the optical constants from tabulated data will not be as accurate. This is especially true for the spectral range around the silicon L-edge and underlines the need to determine optical constants for compound materials.[16] In this regime, the independent atom approximation for the optical constants begins to fail and the electric states of the inner shells are influenced by their neighborhood.[29]

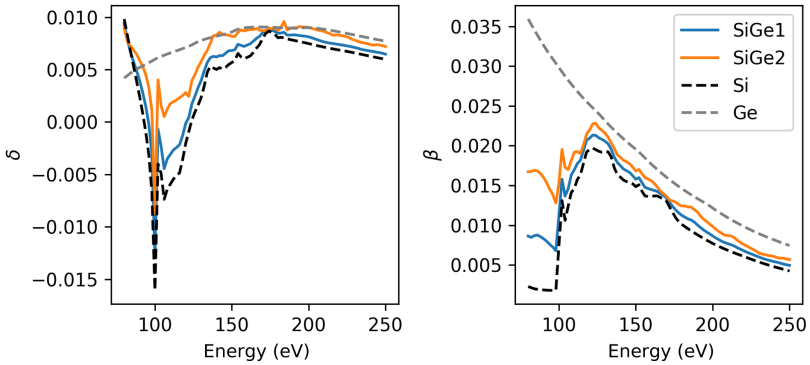

Fig. 5 Optical constants of two variants of SiGe, compared to tabulated data for pure silicon and pure germanium.[24]

Table 1 Comparison of the atomic fraction of germanium in the two SiGe variants.

	Design (%)	X-ray (%)	STEM-EDX (%)
SiGe1	20	17.7	18.7
SiGe2	40	40.3	40.5

5.3 Atomic Fraction of Germanium in the SiGe Layers

Both methods determine the atomic mass fraction of the layers, i.e., they can determine the amount of germanium in the SiGe layers. For STEM-EDX, the quantification is straight-forward, whereas soft X-ray reflectometry depends on the comparison to tabulated data of the optical constants. Table 1 summarizes the atomic fraction of germanium as determined by the two complementary methods versus their design values. We find a good agreement and note that for SiGe1, the atomic fraction of germanium is lower than its design value.

5.4 Comparison with Other Works and Methods

Many other works exist that study the quality of interfaces, especially for semiconductor materials. Often, the focus lies on comparative studies of interfaces with varying quality, such as in Manz et al.,[30] who used a combination of many methods, among them XRR and STEM-EDX, to arrive at the conclusion that they can all be utilized to study the interface sharpness. A similar comparison was done much earlier using Rutherford backscattering and TEM-EDX.[31] Luneville at el.[32] presented a comparison between XRR and EDX for different Cr/Si interfaces, based on the good material contrast for harder X-rays. However, providing a quantitative comparison of different measurement methods is still the exception, as it was usually sufficient to compare trends only. For the fabrication of quantum wells, the precise determination of the extent of intermixing regions is central due to its impact on valley splitting. Just recently, a number of studies were published that use atom probe tomography[4,5] or HR-STEM[2,3] to quantify the interface sharpness of Si/SiGe interfaces, reporting similar values to our work.

6 Summary

We presented a comparative and quantitative study on buried Si/SiGe interfaces investigated using soft X-ray reflectometry and STEM-EDX. The samples feature sub 10 nm thick layers of two variants of SiGe. From the sample wafer, TEM-lamellas were cut for extensive STEM-EDX characterization and other parts were used for soft X-ray reflectometry. We showed that both methods can measure the different layer thicknesses of the complex layer stack and determine the corresponding interface sharpness. We found that both methods generally agree on the measured values, but that the X-ray reflectometry study retrieved slightly sharper interfaces that the STEM-EDX study. The advantages and disadvantages of both methods were discussed

and the investigated sample system was found to be an ideal basis for such a comparison due to its technological relevance, high material quality, and low surface roughness.

7 Appendix A: Data Tables of Optical Constants

List of the optical constants (δ, β) of SiGe1 (Table 2) and SiGe2 (Table 3) as retrieved from the soft X-ray reflectometry measurements. The photon energies $h\nu$ represent the order of measurements, whereas the wavelengths λ are given for reference. The given atomic fraction of germanium stems from the soft X-ray measurement.

Table 2 SiGe1: 17.7% germanium, design: 20.0%

$h\nu$ (eV)	λ (nm)	δ	β
80.0	15.50	0.0094	0.0086
82.0	15.12	0.0079	0.0085
84.0	14.76	0.0067	0.0087
86.0	14.42	0.0058	0.0088
88.0	14.09	0.0049	0.0086
90.0	13.78	0.0040	0.0083
92.0	13.48	0.0028	0.0080
94.0	13.19	0.0015	0.0076
96.0	12.92	−0.0002	0.0072
98.0	12.65	−0.0030	0.0068
100.0	12.40	−0.0128	0.0113
102.0	12.16	−0.0007	0.0158
104.0	11.92	−0.0023	0.0137
106.0	11.70	−0.0045	0.0146
108.0	11.48	−0.0035	0.0163
110.0	11.27	−0.0031	0.0170
112.0	11.07	−0.0027	0.0178
114.0	10.88	−0.0024	0.0182
116.0	10.69	−0.0022	0.0194
118.0	10.51	−0.0013	0.0207
120.0	10.33	−0.0002	0.0210
122.0	10.16	0.0004	0.0213
124.0	10.00	0.0017	0.0213
126.0	9.84	0.0025	0.0210
128.0	9.69	0.0032	0.0208
130.0	9.54	0.0039	0.0206
132.0	9.39	0.0048	0.0202
134.0	9.25	0.0057	0.0195
136.0	9.12	0.0061	0.0186
138.0	8.98	0.0063	0.0179
140.0	8.86	0.0062	0.0175
142.0	8.73	0.0063	0.0171
144.0	8.61	0.0063	0.0169
146.0	8.49	0.0066	0.0166
148.0	8.38	0.0068	0.0162
150.0	8.27	0.0068	0.0158
152.0	8.16	0.0069	0.0160
154.0	8.05	0.0074	0.0154

Table 2 (*Continued*).

$h\nu$ (eV)	λ (nm)	δ	β
156.0	7.95	0.0073	0.0147
158.0	7.85	0.0072	0.0146
160.0	7.75	0.0073	0.0145
162.0	7.65	0.0075	0.0144
164.0	7.56	0.0077	0.0143
166.0	7.47	0.0080	0.0140
168.0	7.38	0.0082	0.0137
170.0	7.29	0.0085	0.0134
172.0	7.21	0.0087	0.0128
174.0	7.13	0.0088	0.0123
176.0	7.04	0.0087	0.0119
178.0	6.97	0.0086	0.0115
180.0	6.89	0.0084	0.0112
182.0	6.81	0.0085	0.0110
184.0	6.74	0.0085	0.0108
186.0	6.67	0.0083	0.0107
188.0	6.59	0.0083	0.0104
190.0	6.53	0.0083	0.0101
192.0	6.46	0.0083	0.0097
194.0	6.39	0.0082	0.0094
196.0	6.33	0.0082	0.0091
198.0	6.26	0.0082	0.0089
200.0	6.20	0.0081	0.0087
202.0	6.14	0.0080	0.0084
204.0	6.08	0.0079	0.0082
206.0	6.02	0.0078	0.0080
208.0	5.96	0.0077	0.0078
210.0	5.90	0.0076	0.0077
212.0	5.85	0.0076	0.0075
214.0	5.79	0.0075	0.0074
216.0	5.74	0.0075	0.0072
218.0	5.69	0.0074	0.0070
220.0	5.64	0.0074	0.0068
222.0	5.58	0.0073	0.0066
224.0	5.54	0.0073	0.0065
226.0	5.49	0.0072	0.0063
228.0	5.44	0.0072	0.0062
230.0	5.39	0.0071	0.0060
232.0	5.34	0.0070	0.0059
234.0	5.30	0.0069	0.0057
236.0	5.25	0.0069	0.0056
238.0	5.21	0.0068	0.0055
240.0	5.17	0.0068	0.0054
242.0	5.12	0.0067	0.0053
244.0	5.08	0.0067	0.0052
246.0	5.04	0.0066	0.0051
248.0	5.00	0.0065	0.0050
250.0	4.96	0.0065	0.0049

Table 3 SiGe2: 40.3% germanium, design: 40.0%

$h\nu$ (eV)	λ (nm)	δ	β
80.0	15.50	0.0089	0.0167
82.0	15.12	0.0077	0.0167
84.0	14.76	0.0073	0.0169
86.0	14.42	0.0069	0.0168
88.0	14.09	0.0065	0.0165
90.0	13.78	0.0059	0.0160
92.0	13.48	0.0053	0.0153
94.0	13.19	0.0045	0.0145
96.0	12.92	0.0033	0.0138
98.0	12.65	0.0011	0.0128
100.0	12.40	−0.0087	0.0153
102.0	12.16	0.0040	0.0195
104.0	11.92	0.0016	0.0173
106.0	11.70	0.0005	0.0170
108.0	11.48	0.0012	0.0181
110.0	11.27	0.0017	0.0192
112.0	11.07	0.0019	0.0193
114.0	10.88	0.0021	0.0190
116.0	10.69	0.0023	0.0201
118.0	10.51	0.0025	0.0215
120.0	10.33	0.0028	0.0220
122.0	10.16	0.0024	0.0227
124.0	10.00	0.0039	0.0228
126.0	9.84	0.0045	0.0222
128.0	9.69	0.0052	0.0219
130.0	9.54	0.0057	0.0216
132.0	9.39	0.0063	0.0211
134.0	9.25	0.0068	0.0204
136.0	9.12	0.0075	0.0196
138.0	8.98	0.0082	0.0189
140.0	8.86	0.0083	0.0185
142.0	8.73	0.0086	0.0182
144.0	8.61	0.0084	0.0180
146.0	8.49	0.0083	0.0177
148.0	8.38	0.0083	0.0173
150.0	8.27	0.0082	0.0168
152.0	8.16	0.0081	0.0170
154.0	8.05	0.0085	0.0165
156.0	7.95	0.0088	0.0160
158.0	7.85	0.0087	0.0158
160.0	7.75	0.0088	0.0156
162.0	7.65	0.0088	0.0153
164.0	7.56	0.0088	0.0148
166.0	7.47	0.0089	0.0143
168.0	7.38	0.0088	0.0140
170.0	7.29	0.0087	0.0136

Table 3 (*Continued*).

$h\nu$ (eV)	λ (nm)	δ	β
172.0	7.21	0.0087	0.0132
174.0	7.13	0.0089	0.0130
176.0	7.04	0.0089	0.0129
178.0	6.97	0.0089	0.0126
180.0	6.89	0.0087	0.0124
182.0	6.81	0.0090	0.0124
184.0	6.74	0.0096	0.0123
186.0	6.67	0.0088	0.0123
188.0	6.59	0.0089	0.0120
190.0	6.53	0.0090	0.0117
192.0	6.46	0.0090	0.0112
194.0	6.39	0.0091	0.0108
196.0	6.33	0.0091	0.0105
198.0	6.26	0.0090	0.0101
200.0	6.20	0.0090	0.0098
202.0	6.14	0.0089	0.0095
204.0	6.08	0.0088	0.0092
206.0	6.02	0.0087	0.0090
208.0	5.96	0.0087	0.0087
210.0	5.90	0.0086	0.0087
212.0	5.85	0.0085	0.0087
214.0	5.79	0.0084	0.0084
216.0	5.74	0.0083	0.0081
218.0	5.69	0.0083	0.0079
220.0	5.64	0.0083	0.0076
222.0	5.58	0.0082	0.0074
224.0	5.54	0.0082	0.0072
226.0	5.49	0.0081	0.0070
228.0	5.44	0.0079	0.0068
230.0	5.39	0.0078	0.0065
232.0	5.34	0.0077	0.0064
234.0	5.30	0.0076	0.0063
236.0	5.25	0.0075	0.0062
238.0	5.21	0.0075	0.0061
240.0	5.17	0.0074	0.0061
242.0	5.12	0.0073	0.0059
244.0	5.08	0.0074	0.0058
246.0	5.04	0.0073	0.0059
248.0	5.00	0.0073	0.0058
250.0	4.96	0.0072	0.0057

Code and Data Availability

Company proprietary information will not be made available, but manuscript content is consistent with JM3 technical content guidelines. The data that support the findings of this article can be requested from the author at richard.ciesielski@ptb.de.

Acknowledgments

The project is supported by Chips Joint Undertaking (Grant No. 101096772) - 14ACMOS and (Grant No. 875999) - IT2 and its members, including the top-up funding of Belgium and the Netherlands, as well as from the EMPIR programme 20IND04 ATMOC. We wish to thank Qais Saadeh and Gavin Phillips for valuable discussions.

References

1. H. Xiao, *3D IC Devices, Technologies, and Manufacturing*, SPIE Press, Bellingham, Washington (2016).
2. D. Degli Esposti et al., "Low disorder and high valley splitting in silicon," *NPJ Quantum Inf.* **10**(1), 32 (2024).
3. Y. Shimura et al., "Compressively strained epitaxial Ge layers for quantum computing applications," *Mater. Sci. Semicond. Process.* **174**, 108231 (2024).
4. O. Dyck et al., "Accurate quantification of Si/SiGe interface profiles via atom probe tomography," *Adv. Mater. Interfaces* **4**(21), 1700622 (2017).
5. B. Paquelet Wuetz et al., "Atomic fluctuations lifting the energy degeneracy in Si/SiGe quantum dots," *Nat. Commun.* **13**(1), 7730 (2022).
6. P. Schuddinck et al., "PPAC of sheet-based CFET configurations for 4 track design with 16 nm metal pitch," in *IEEE Symp. VLSI Technol. and Circuits (VLSI Technol. and Circuits)*, IEEE, pp. 365–366 (2022).
7. R. Ciesielski et al., "Soft X-ray reflectometry for the inspection of interlayer roughness in stacked thin film structures," *Proc. SPIE* **12955**, 1295507 (2024).
8. Y. M. Haddara, P. Ashburn, and D. M. Bagnall, "Silicon-germanium: properties, growth and applications," in *Springer Handbook of Electronic and Photonic Materials*, P. C. Safa Kasap, Ed., Springer (2017).
9. G. Burkard et al., "Semiconductor spin qubits," *Rev. Mod. Phys.* **95**(2), 025003 (2023).
10. S. Subramanian et al., "First monolithic integration of 3D complementary FET (CFET) on 300 mm wafers," in *IEEE Symp. VLSI Technol.*, IEEE, pp. 1–2 (2020).
11. "Imec puts complementary FET (CFET) on the logic technology roadmap," (2022). https://www.imec-int.com/en/articles/imec-puts-complementary-fet-cfet-logic-technology-roadmap (accessed 14 June 2024).
12. R. Loo et al., "Epitaxial SiGe/Si multi-stacks for complementary FET devices," in *Int. Conf. Solid State Devices and Mater. (SSDM), F-5-03* (2023).
13. F. Scholze, J. Tümmler, and G. Ulm, "High-accuracy radiometry in the EUV range at the PTB soft x-ray beamline," *Metrologia* **40**(1), S224 (2003).
14. F. Scholze et al., "Status of EUV reflectometry at PTB," *Proc. SPIE* **5751**, 749–758 (2005).
15. N. Koster et al., "Molecular contamination mitigation in EUVL by environmental control," *Microelectron. Eng.* **61**, 65–76 (2002).
16. R. Ciesielski et al., "Determination of optical constants of thin films in the EUV," *Appl. Opt.* **61**(8), 2060–2078 (2022).
17. Q. Saadeh et al., "Validation of optical constants in the EUV spectral range," *Proc. SPIE* **11147**, 111471P (2019).
18. Q. Saadeh et al., "Time-frequency analysis assisted determination of ruthenium optical constants in the sub-EUV spectral range 8 nm–23.75 nm," *Opt. Express* **29**(25), 40993–41013 (2021).
19. M. Bass et al., *Handbook of Optics, Volume I: Geometrical and Physical Optics, Polarized Light, Components and Instruments*, 3rd ed., McGraw-Hill, Inc. (2009).
20. L. Nevot and P. Croce, "Caractérisation des surfaces par réflexion rasante de rayons X. Application à l'étude du polissage de quelques verres silicates," *Rev. Phys. Appl.* **15**(3), 761–779 (1980).
21. G. Vignaud and A. Gibaud, "REFLEX: a program for the analysis of specular X-ray and neutron reflectivity data," *J. Appl. Crystallogr.* **52**(1), 201–213 (2019).
22. D. Stearns, "The scattering of X rays from nonideal multilayer structures," *J. Appl. Phys.* **65**(2), 491–506 (1989).
23. M. Wormington, "Evidence for grading at polished surfaces from grazing-incidence X-ray scattering," *Philos. Mag. Lett.* **74**(3), 211–216 (1996).
24. B. L. Henke, E. Gullikson, and J. Davis, "X-ray interactions: photoabsorption, scattering, transmission and reflection E = 50-30,000 eV, Z = 1-92," *At. Data Nucl. Data Tables* **54**(2), 181–342 (1993).
25. C. Zhu et al., "Algorithm 778: L–BFGS–B: Fortran subroutines for large–scale bound–constrained optimization," *ACM Trans. Math. Softw.* **23**(4), 550–560 (1997).
26. P. Virtanen et al., "SciPy 1.0: fundamental algorithms for scientific computing in Python," *Nat. Methods* **17**(3), 261–272 (2020).
27. J. Goodman and J. Weare, "Ensemble samplers with affine invariance," *Commun. App. Math. Comput. Sci.* **5**(1), 65–80 (2010).
28. D. Foreman-Mackey et al., "emcee: the MCMC hammer," *Publ. Astron. Soc. Pac.* **125**(925), 306 (2013).

29. Q. Saadeh, "Bayesian inferences and time-frequency analysis assisted determination of optical constants in the extreme ultraviolet range," PhD thesis, TU Berlin (2023).
30. C. Manz et al., "Improved AlScN/GaN heterostructures grown by metal-organic chemical vapor deposition," *Semicond. Sci. Technol.* **36**(3), 034003 (2021).
31. A. Markwitz et al., "Depth profile analysis: STEM-EDX vs. RBS," *Surf. Interface Anal.* **26**(5), 359–366 (1998).
32. L. Luneville et al., "Interdiffusion processes at irradiated Cr/Si interfaces," *J. Alloys Compd.* **626**, 65–69 (2015).

Biographies of the authors are not available.